Chemical Science

ROYAL SOCIETY OF CHEMISTRY

EDGE ARTICLE

View Article Online
View Journal | View Issue

Check for updates

Cite this: *Chem. Sci.*, 2020, **11**, 7144

All publication charges for this article have been paid for by the Royal Society of Chemistry

Open Access Article. Published on 12 June 2020. Downloaded on 1/23/2025 2:37:06 PM.
This article is licensed under a Creative Commons Attribution-NonCommercial 3.0 Unported Licence.

Selective oxo ligand functionalisation and substitution reactivity in an oxo/catecholate-bridged U^{IV}/U^{IV} Pacman complex†

Bradley E. Cowie, [a] Iskander Douair,[b] Laurent Maron, [b] Jason B. Love *[a] and Polly L. Arnold ‡*[a]

The oxo- and catecholate-bridged U^{IV}/U^{IV} Pacman complex [{(py)U^{IV}OU^{IV}(μ-$O_2C_6H_4$)(py)}(L^A)] **A** (L^A = a macrocyclic "Pacman" ligand; anthracenylene hinge between N_4-donor pockets, ethyl substituents on *meso*-carbon atom of each N_4-donor pocket) featuring a bent U^{IV}–O–U^{IV} oxo bridge readily reacts with small molecule substrates to undergo either oxo-atom functionalisation or substitution. Complex **A** reacts with H_2O or MeOH to afford [{(py)U^{IV}(μ-OH)$_2U^{IV}$(μ-$O_2C_6H_4$)(py)}(L^A)] (**1**) and [{(py)U^{IV}(μ-OH)(μ-OMe)U^{IV}(μ-$O_2C_6H_4$)(py)}(L^A)] (**2**), respectively, in which the bridging oxo ligand in **A** is substituted for two bridging hydroxo ligands or one bridging hydroxo and one bridging methoxy ligand, respectively. Alternatively, **A** reacts with either 0.5 equiv. of S_8 or 4 equiv. of Se to provide [{(py)U^{IV}(μ-η^2:η^2-E_2)U^{IV}(μ-$O_2C_6H_4$)(py)}(L^A)] (E = S (**3**), Se (**4**)) respectively, in which the $[E_2]^{2-}$ ion bridges the two U^{IV} centres. To the best of our knowledge, complex **A** is the first example of either a d- or f-block bimetallic μ-oxo complex that activates elemental chalcogens. Complex **A** also reacts with XeF_2 or 2 equiv. of Me_3SiCl to provide [{(py)U^{IV}(μ-X)$_2U^{IV}$(μ-$O_2C_6H_4$)(py)}(L^A)] (X = F (**5**), Cl (**6**)), in which the oxo ligand has been substituted for two bridging halido ligands. Reacting **A** with either XeF_2 or Me_3SiCl in the presence of O(Bcat)$_2$ at room temperature forms [{(py)U^{IV}(μ-X)(μ-OBcat)U^{IV}(μ-$O_2C_6H_4$)(py)}(L^A)] (X = F (**5A**), Cl (**6A**)), which upon heating to 80 °C is converted to **5** and **6**, respectively. In order to probe the importance of the bent U^{IV}–O–U^{IV} motif in **A** on the observed reactivity, the bis(boroxido)-U^{IV}/U^{IV} complex, [{(py)(pinBO)U^{IV}OU^{IV}(OBpin)(py)}(L^A)] (**B**), featuring a linear U^{IV}–O–U^{IV} bond angle was treated with H_2O and Me_3SiCl. Complex **B** reacts with two equiv. of either H_2O or Me_3SiCl to provide [{(py)HOU^{IV}OU^{IV}OH(py)}(L^A)] (**7**) and [{(py)ClOU^{IV}OU^{IV}Cl(py)}(L^A)] (**8**), respectively, in which reactions occur preferentially at the boroxido ligands, with the μ-oxo ligand unchanged. The formal U^{IV} oxidation state is retained in all of the products **1**–**8**, and selective reactions at the bridging oxo ligand in **A** is facilitated by: (1) its highly nucleophilic character which is a result of a non-linear U^{IV}–O–U^{IV} bond angle causing an increase in U–O bond covalency and localisation of the lone pairs of electrons on the μ-oxo group, and (2) the presence of the bridging catecholate ligand, which destabilises a linear oxo-bridging geometry and stabilises the resulting products.

Received 23rd April 2020
Accepted 11th June 2020

DOI: 10.1039/d0sc02297g

rsc.li/chemical-science

Introduction

Molecular U^{III} complexes are renowned for activating small molecules due their Lewis acidity, the accessibility of the U^{III} → U^{IV} redox couple and in some cases, the capacity for U^{III} to back-donate into empty ligand-based molecular orbitals.[1–3] For example, it was demonstrated in the 1980s that [U^{III}(η^5-$C_5H_4R)_3$] (R = Me, $SiMe_3$) reacted with half an equivalent of CS_2 to form [{U^{IV}(η^5-$C_5H_4R)_3$}$_2$(μ-η^1:η^2-CS_2)] through U^{III} → U^{IV} oxidation (Fig. 1A).[4] Since then, a plethora of examples of low oxidation state uranium complexes for the activation of small molecules such as NO, N_3^-, C_xH_y hydrocarbons, S_8 and Se have been characterised,[5,6] such as a recently reported example of the use of a U^{III}/U^{III} dimer from our research group, [{U^{III}($OBMes_2$)$_3$}$_2$], which reacts with S_8 to provide [{U^{V}($OBMes_2$)$_3$}$_2$(μ-η^2:η^2-S_2)$_2$] (Fig. 1B).[7] A variety of U^{IV}–O–U^{IV} containing complexes with many different supporting ligands have also been formed, since this is normally a thermodynamic

[a]*EaStCHEM School of Chemistry, The University of Edinburgh, Joseph Black Building, The King's Buildings, Edinburgh, EH9 3FJ, UK*

[b]*Université de Toulouse, INSA, UPS, CNRS, UMR 5215, LPCNO, 135 Avenue de Rangueil, F-31077 Toulouse, France*

† Electronic supplementary information (ESI) available. CCDC 1984900–1984907. For ESI and crystallographic data in CIF or other electronic format see DOI: 10.1039/d0sc02297g

‡ Current address: Department of Chemistry, University of California, Berkeley, CA 94720, USA; Chemical Sciences Division, Lawrence Berkeley National Laboratory, Berkeley, CA94720, USA. pla@berkeley.edu

This journal is © The Royal Society of Chemistry 2020

Open Access Article. Published on 12 June 2020. Downloaded on 1/23/2025 2:37:06 PM.
This article is licensed under a Creative Commons Attribution-NonCommercial 3.0 Unported Licence.

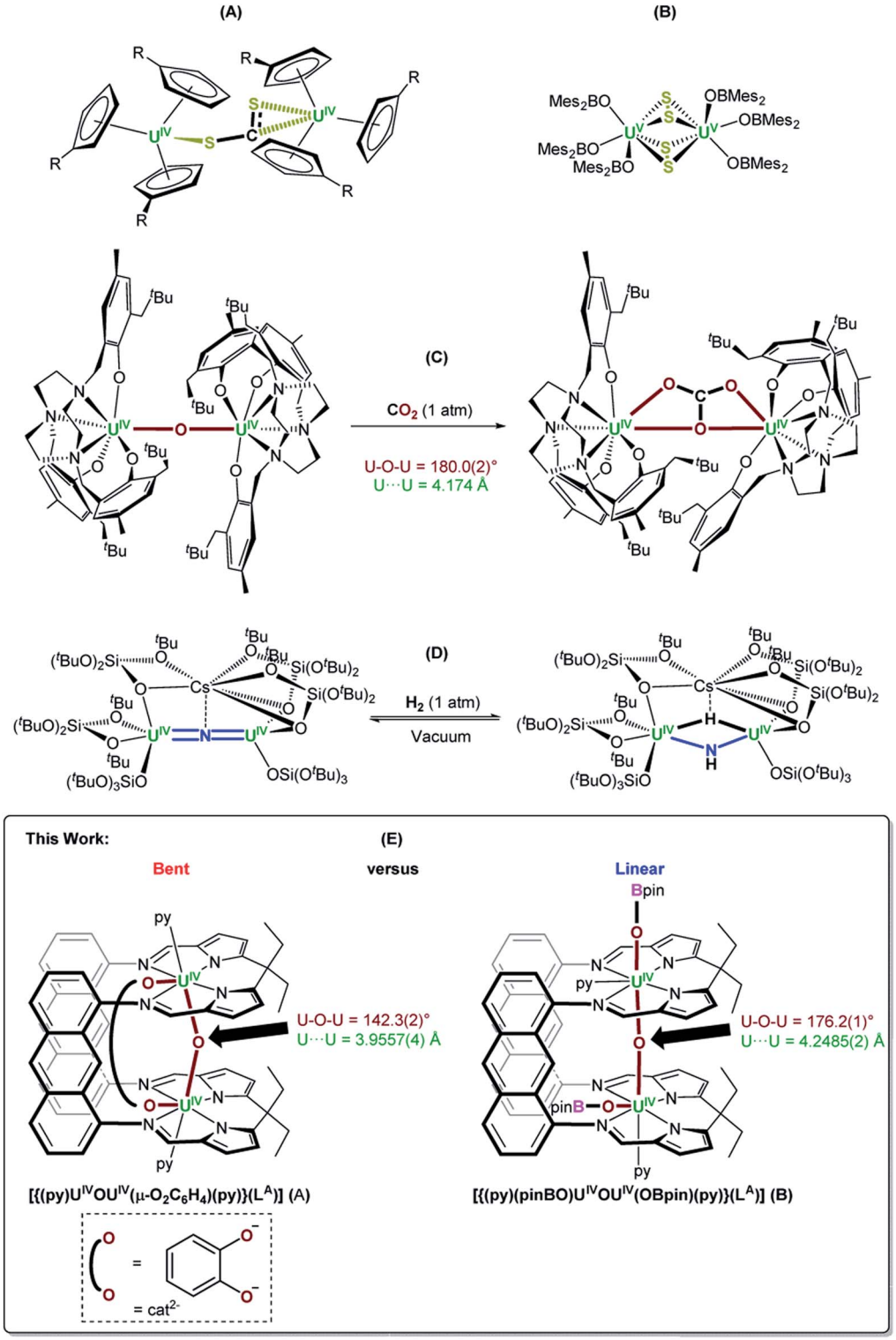

Fig. 1 (A) and (B) Examples of CS_2 and S_8 activation by molecular U^{III} complexes, respectively.[4,7] (C) and (D) Examples of functionalisation of oxo and nitride ligands bridging between two U^{IV} centres, respectively.[14,17] (E) The bent, oxo-/catecholate-bridged U^{IV}/U^{IV} Pacman complex, [{(py)$U^{IV}OU^{IV}$(μ-$O_2C_6H_4$)(py)}(L^A)] (**A**), and the linear, oxo-bridged bis(boroxido)-U^{IV}/U^{IV} Pacman complex, [{(py)(pinBO)$U^{IV}OU^{IV}$(OBpin)(py)}(L^A)] (**B**);[18] a comparison of their reactivity with a variety of small molecule reagents is presented in this work (py = pyridine).

sink. Such complexes are commonly formed either by treating 2 equiv. of a U^{III} complex with an oxo source such as N_2O, or half an equiv. of CO_2.[6]

Small molecule activation by molecular U^{IV} and U^{V} complexes is exceedingly rare and difficult to predict or design. The U^{IV} centre is significantly less reducing and relatively inert to further

Open Access Article. Published on 12 June 2020. Downloaded on 1/23/2025 2:37:06 PM. This article is licensed under a Creative Commons Attribution-NonCommercial 3.0 Unported Licence.

redox processes.[8–11] The functionalisation of a bridging oxo ligand between two U^{IV} centres is still very rare as the U–O bond is very strong; the single U–O bond in $[Cp'_2U^{IV}O]$ (Cp' = C_5H_2-1,2,4-$^tBu_3$) is 293 kJ mol^{-1} stronger than the double U=NMe bond in $[Cp'_2U^{IV}NMe]$.[6,12,13] However, under the right circumstances the single-atom bridged U^{IV}–E–U^{IV} unit can hold a privileged position. Such examples are limited to the conversion of the μ-oxo group into a bridging $[CO_3]^-$ ligand by treatment with CO_2, such as in the conversion of $[\{((^{Neop,Me}ArO)_3tacn)U^{IV}\}_2(\mu\text{-}O)]$ ($(^{Neop,Me}ArOH)_3tacn$ = 1,4,7-tris(2-hydroxy-5-methyl-3-neopentylbenzyl)-1,4,7-triazacyclononane) into $[\{((^{Neop,Me}ArO)_3tacn)U^{IV}\}_2(\mu\text{-}CO_3)]$ (Fig. 1C).[6,14] Further functionalisation of a U^{IV}-coordinated, activated small molecule fragment typically requires the use of highly reactive external reagents.[15] A bridging nitrido ligand in $[U^{IV}{=}N{=}U^{IV}]$ complexes is amenable to functionalisation, such as the conversion of $[Cs\{U^{IV}\{OSi(O^tBu)_3\}_3\}_2(\mu\text{-}N)]$ (synthesised from $[U^{III}\{OSi(O^tBu)_3\}_3]_2$ and CsN_3)[16] into $[Cs\{U^{IV}\{OSi(O^tBu)_3\}_3\}_2(\mu\text{-}NH)(\mu\text{-}H)]$ by treatment with H_2 (Fig. 1D).[17] The design principles that enable this reactivity from such a fragment are not yet clear.

Here we report the remarkably different reactivity shown by two very similar U^{IV}/U^{IV} μ-oxo complexes of the macrocyclic "Pacman" ligand L^A, Fig. 1E. Complex **A** $[\{(py)U^{IV}OU^{IV}(\mu\text{-}O_2C_6H_4)(py)\}(L^A)]$ is found to be reactive towards small molecules and has a catecholate ligand that bridges the U–O–U unit giving a short, yet bent U–O–U angle of 142.3(3)° and a U···U separation of 3.9557(4) Å. In contrast, the parent complex **B** $[\{(py)(pinBO)U^{IV}OU^{IV}(OBpin)(py)\}(L^A)]$ is unreactive, has a longer U···U separation of 4.2485(2) Å and a more 'normal' linear U–O–U angle of 176.2(1)° (Fig. 1E).[18]

Results

A. Reactivity of a bent oxo/catecholato-bridged U^{IV}/U^{IV} Pacman complex

We previously reported the synthesis of $[\{(py)U^{IV}OU^{IV}(\mu\text{-}O_2C_6H_4)(py)\}(L^A)]$ (**A**) by reaction of the bis(uranyl) Pacman complex, $[\{U^{VI}O_2(py)\}_2(L^A)]$,[19,20] with 3 equiv. of B_2cat_2 (Scheme 1).[18] We have now found that **A** reacts with weak acids such as H_2O and MeOH, either stoichiometrically (1 equiv.) or in excess (35 equiv. H_2O or 5 equiv. MeOH) to provide $[\{(py)U^{IV}(\mu\text{-}OH)_2U^{IV}(\mu\text{-}O_2C_6H_4)(py)\}(L^A)]$ (**1**) and $[\{(py)U^{IV}(\mu\text{-}OMe)(\mu\text{-}OH)U^{IV}(\mu\text{-}O_2C_6H_4)(py)\}(L^A)]$ (**2**) as yellow solids in 73 and 54% isolated yield, respectively (Scheme 1). We have previously reported another uranium hydroxide supported by the Pacman ligand, $[\{U^VO(OH)(py)\}(H_2L^{Me})]$ (H_4L^{Me} = Pacman-shaped macrocyclic Schiff-base ligand with methyl substituents on the *meso*-carbon atoms and a dimethylphenylene hinge). In that case it was formed by treating an oxo-lithiated uranyl(V) complex, $[\{U^VO\{OLi(py)_3\}(py)\}(LiHL^{Me})]$, with 2 equiv. of HCl.[21] In **1**, the bridging oxo ligand in **A** has been formally substituted by two bridging hydroxo ligands in a complex that has C_{2h} symmetry according to the 13 paramagnetically shifted resonances between 95.5 and −36.1 ppm in the ^{1}H NMR spectrum at 300 K.

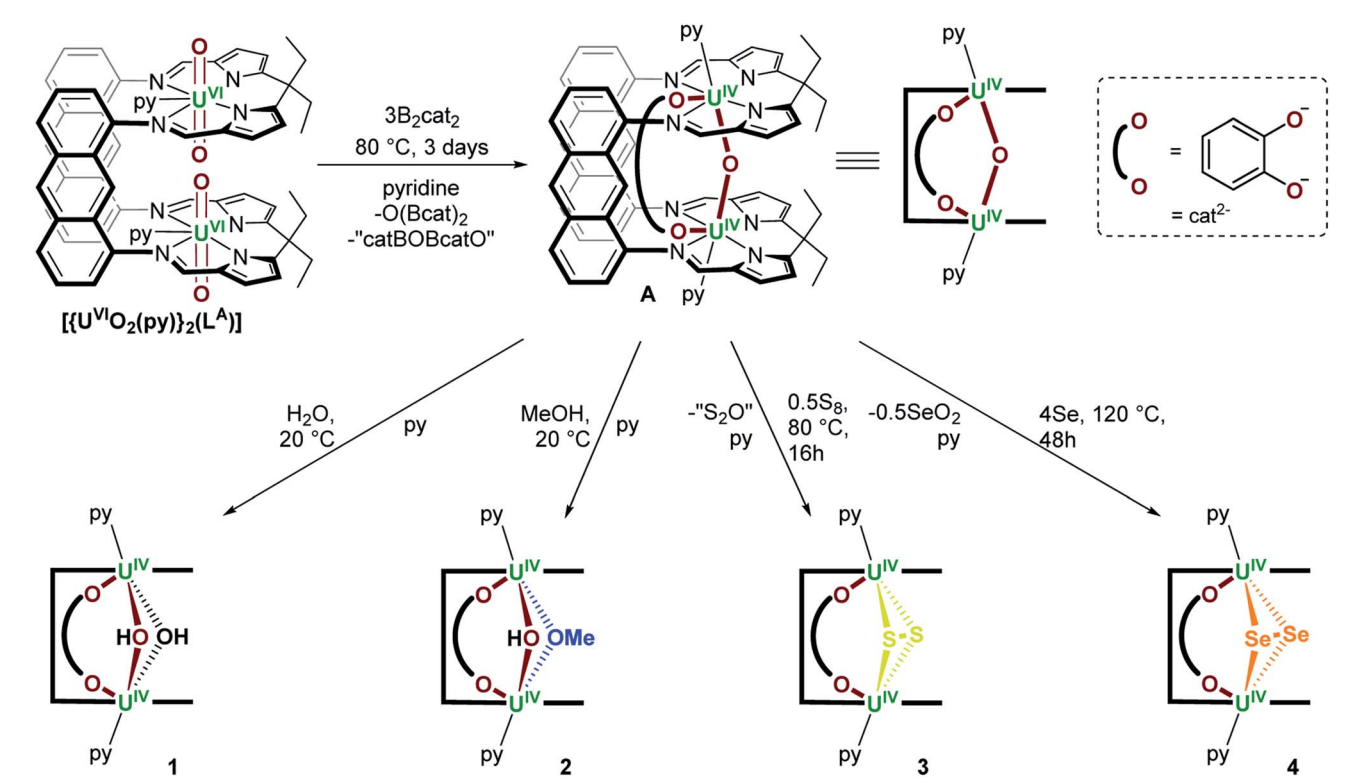

Scheme 1 Synthesis of $[\{(py)U^{IV}OU^{IV}(\mu\text{-}O_2C_6H_4)(py)\}(L^A)]$ (**A**) from $[\{U^{VI}O_2(py)\}_2(L^A)]$ and 3 equiv. of B_2cat_2,[18] and subsequent synthesis of $[\{(py)U^{IV}(\mu\text{-}OH)_2U^{IV}(\mu\text{-}O_2C_6H_4)(py)\}(L^A)]$ (**1**), $[\{(py)U^{IV}(\mu\text{-}OMe)(\mu\text{-}OH)U^{IV}(\mu\text{-}O_2C_6H_4)(py)\}(L^A)]$ (**2**) and $[\{(py)U^{IV}(\mu\text{-}\eta^2\text{:}\eta^2\text{-}E_2)U^{IV}(\mu\text{-}O_2C_6H_4)(py)\}(L^A)]$ (E = S (**3**), Se (**4**)); py = pyridine.

 This journal is © The Royal Society of Chemistry 2020

Open Access Article. Published on 12 June 2020. Downloaded on 1/23/2025 2:37:06 PM.
This article is licensed under a Creative Commons Attribution-NonCommercial 3.0 Unported Licence.

In contrast, complex **2** possesses C_{1v} symmetry with one bridging methoxy and one bridging hydroxo ligand between the two U centres. While 21 resonances are recorded in the ^{1}H NMR spectra at either 300 K (96.65 to −35.89 ppm) or 360 K (78.48 to −27.28 ppm), the resonances for **2** are significantly sharper at elevated temperatures, suggesting dynamic behaviour of the bridging ligands in solution. The μ-O*H* resonance in both **1** and **2** could not be located in the ^{1}H NMR spectra, but we note that it is close to the two paramagnetic cations and so would be significantly shifted and broadened.

Complex **A** also reacts with 0.5 equiv. of S_8 over the course of 16 hours at 80 °C to afford [{(py)U^{IV}(μ-η^2:η^2-S$_2$)U^{IV}(μ-O$_2$C$_6$H$_4$)(py)}(L^A)] (**3**) as a brown/yellow solid in 55% isolated yield (Scheme 1); in this case the bridging oxo ligand has been substituted for an $[S_2]^{2-}$ ligand. During this reaction, the μ-oxo ligand is likely lost as S_2O, which is unstable and expected to ultimately form SO_2 and S_8, meaning that no change in uranium oxidation state is needed.[22] Complex **3** may also be obtained by reacting **A** with a slight excess of CS_2 (∼3 equiv.) and heating to 120 °C for 4 days. This reaction does not require any redox change in the metal or ligands if the by-product is COS. Also, no further reaction is seen with an excess of S_8. The ^{1}H NMR spectrum of **3** contains 12 resonances between 62.24 and −40.90 ppm, indicative of a U^{IV}/U^{IV} complex of C_{2h} symmetry.

Additionally, **A** reacts with four or more equiv. of elemental selenium when heated to 125 °C for 48 hours in pyridine to provide [{(py)U^{IV}(μ-η^2:η^2-Se$_2$)U^{IV}(μ-O$_2$C$_6$H$_4$)(py)}(L^A)] (**4**) as a red/brown solid in 43% yield (Scheme 1). The ^{1}H NMR

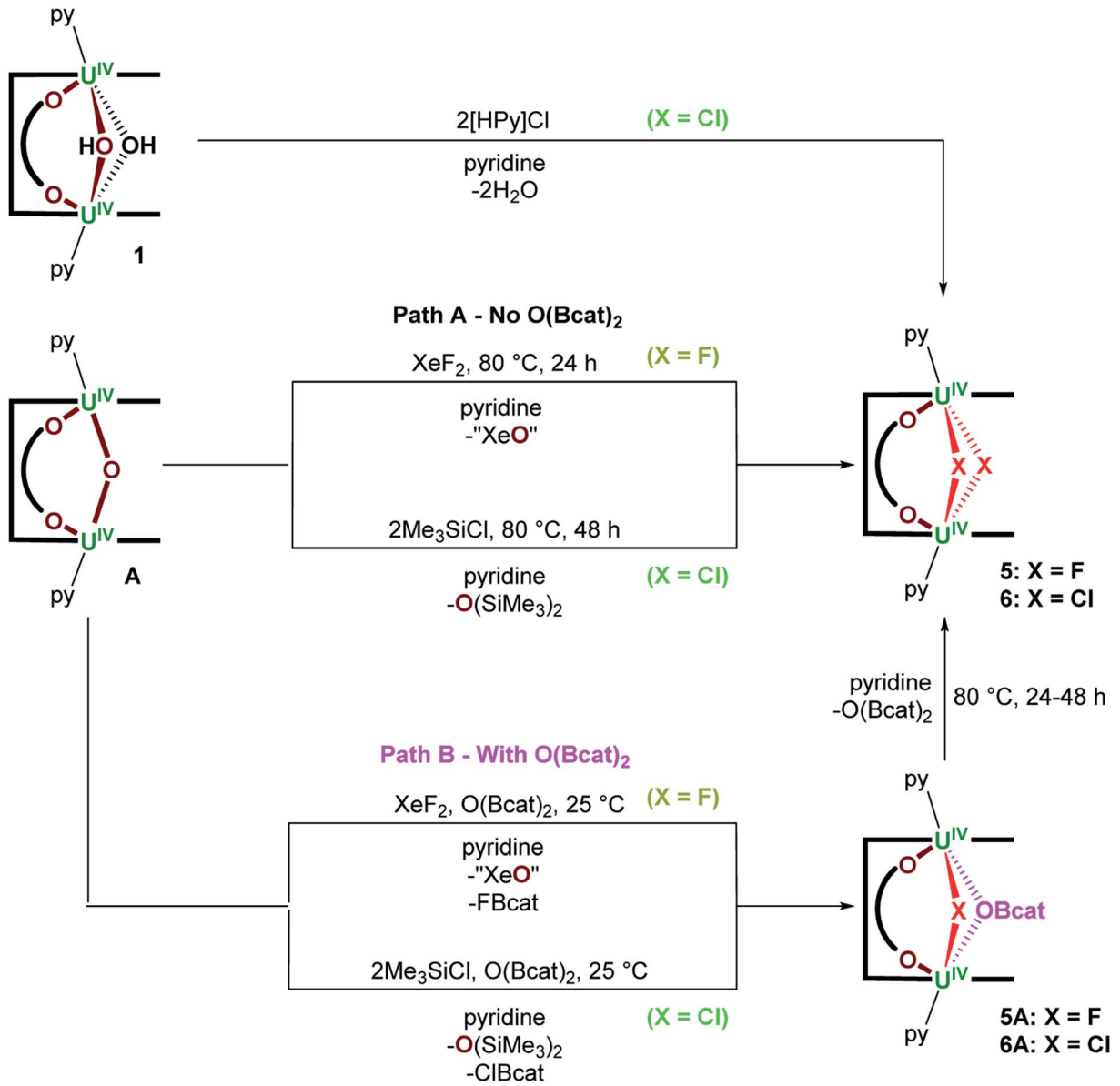

Scheme 2 Synthesis of [{(py)U^{IV}(μ-X)$_2$U^{IV}(μ-O$_2$C$_6$H$_4$)(py)}(L^A)] (X = F (**5**), Cl (**6**)) from (A) **A** and XeF_2 or Me_3SiCl, respectively. (B) In the presence of 1 equiv. of O(Bcat)$_2$ **A** reacts with XeF_2 or Me_3SiCl to afford [{(py)U^{IV}(μ-X)(μ-OBcat)U^{IV}(μ-O$_2$C$_6$H$_4$)(py)}(L^A)] (X = F (**5A**), Cl (**6A**)), which can be converted into **5** and **6** by heating pyridine solutions of the reaction mixtures at 80 °C for 24 and 48 hours, respectively.

Open Access Article. Published on 12 June 2020. Downloaded on 1/23/2025 2:37:06 PM.
This article is licensed under a Creative Commons Attribution-NonCommercial 3.0 Unported Licence.

spectrum of **4** contains 15 resonances between 62.49 and −41.70 ppm. The formation of complex **4** involves substitution of the bridging oxo ligand in **A** for a bridging $[Se_2]^{2-}$ ligand and presumably formation of Se_2O as the by-product. In an attempt to prepare the mono-Se adduct $[\{(py)U^{IV}SeU^{IV}(\mu\text{-}O_2C_6H_4)(py)\}(L^A)]$, **A** was treated with one equivalent of the potent chalcogen atom transfer reagent, $Ph_3P{=}Se$.[23] However no reaction occurred (see Discussion section). Furthermore, complex **A** does not react with elemental tellurium, P_4, Ph_2Se_2 or Ph_2Te_2.

A reaction between **A** and XeF_2, designed to target a U^V/U^V product containing the $[FU^VOU^VF]^{6+}$ unit, instead forms the U^{IV}/U^{IV} bridging bis(fluorido) complex, $[\{(py)U^{IV}(\mu\text{-}F)_2U^{IV}(\mu\text{-}O_2C_6H_4)(py)\}(L^A)]$ (**5**), following heating the reaction mixture at 80 °C for 24 hours (Scheme 2 Path A); no reaction occurs at room temperature. Complex **5** is formed by substitution of the bridging oxo ligand in **A** for two bridging fluorido ligands and was isolated as a lemon yellow solid in 40% yield; the formal by-product XeO is unstable so a mixture of XeO_n ($n = 2$ or 3) and Xe gas likely results.[24] The ^{1}H NMR spectrum of **5** at 300 K contains 11 resonances from 64.89 to −55.51 ppm, while that recorded at 360 K contains the anticipated 14 resonances (88.91 to −43.00 ppm) for a C_{2h} symmetric product. No resonances were seen in the ^{19}F NMR spectrum which may be due to a dynamic process rather than proximity to the paramagnetic U centres since a resonance is observed for **5A** below.

If the $O(Bcat)_2$ by-product produced during the formation of **A** from $[\{U^{VI}O_2(py)\}_2(L^A)]$ and 3 equiv. of B_2cat_2 (Scheme 1) is not removed from the product mixture, a different product is initially formed in the reaction with XeF_2. From reactions of **A** with 1 equiv. of $O(Bcat)_2$ and XeF_2 at room temperature, the mixed–bridged complex, $[\{(py)U^{IV}(\mu\text{-}F)(\mu\text{-}OBcat)U^{IV}(\mu\text{-}O_2C_6H_4)(py)\}(L^A)]$ (**5A**; Scheme 2 Path B), can be isolated in 68% yield. In **5A** the bridging oxo ligand has been substituted by a bridging fluorido and bridging catecholatoboroxido ligand. Heating **5A** to 80 °C overnight results in complete conversion to the $[U^{IV}{-}F_2{-}U^{IV}]$ complex **5** (Scheme 2). The by-products formed alongside **5A** are presumed to be FBcat and "XeO", the former of which then reacts at higher temperature to afford **5** and $O(Bcat)_2$ (Scheme 2). Complex **5A** is characterised by a chemical shift of 141 ppm in the ^{19}F NMR spectrum, 13 resonances located between 102.25 and −38.01 ppm in the ^{1}H NMR spectrum at 300 K and 25 resonances between 81.60 and −42.64 ppm at 360 K. Unfortunately, no resonances are seen in the ^{11}B NMR spectrum.

To the best of our knowledge, the conversion of a bimetallic μ-oxo complex into a bimetallic μ-fluorido complex without a change in metal oxidation state using XeF_2 is unprecedented in either d- or f-block chemistry. The conversion of a μ-oxo ligand in **A** into two μ-fluorido ligands in **5**, or μ-fluorido/μ-boroxido ligands in **5A** is likely thermodynamically driven, as

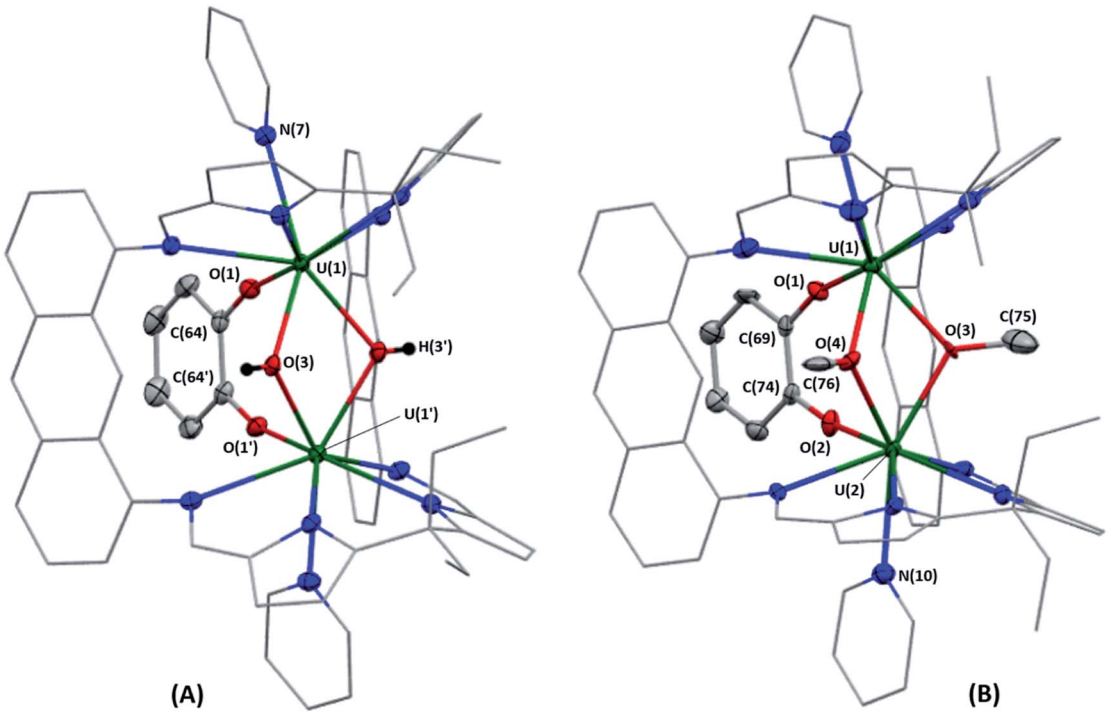

Fig. 2 Solid-state structures of **1·3THF** (A) and **2-OMe/OH·C$_6$H$_6$** (B). Displacement ellipsoids are drawn with 50% probability, and carbon atoms of L^A and U-coordinated solvent molecules drawn wireframe. For clarity, hydrogen atoms (except for H(3) and H(3′) of **1·3THF**), lattice solvent and the lower-fractional occupancy disordered components of **1·3THF** (C(10)) and **2-OMe/OH·C$_6$H$_6$** (C(8)) are omitted. Furthermore, C(76) of **2-OMe/OH·C$_6$H$_6$** possesses partial occupancy (0.69). Selected bond lengths [Å] and bond angles [°] for **1·3THF**: U(1)–O(1), 2.139(3); U(1)–O(3), 2.325(3); U(1)–O(3′), 2.322(3); O(1)–C(64), 1.340(5); U(1)···U(1′), 3.7696(3); U(1)–O(3)–U(1′), 108.4(1). Selected bond lengths [Å] and angles [°] for **2-OMe/OH·C$_6$H$_6$**: U(1)–O(1), 2.112(4); U(1)–O(3), 2.358(5); U(1)–O(4), 2.345(4); U(2)–O(2), 2.113(4); U(2)–O(3), 2.347(4); U(2)–O(4), 2.379(4); O(1)–C(69), 1.362(7); O(2)–C(74), 1.368(7); O(3)–C(75), 1.429(9); O(4)–C(76), 1.47(1); U(1)···U(2), 3.7763(5); U(1)–O(3)–U(2), 106.8(2); U(1)–O(4)–U(2), 106.2(2).

 This journal is © The Royal Society of Chemistry 2020

Open Access Article. Published on 12 June 2020. Downloaded on 1/23/2025 2:37:06 PM.
This article is licensed under a Creative Commons Attribution-NonCommercial 3.0 Unported Licence.

the coordination of two μ-X^- ligands would provide increased π-donation to the U^{IV} centres and account for the decrease in π-donation from the bent U–O–U oxo ligand (see DFT calculations in the Discussion section below).

Lastly, **A** reacts with 2 equiv. of Me_3SiCl at 80 °C over the course of 48 hours to provide [{(py)U^{IV}(μ-Cl)$_2$$U^{IV}$(μ-$O_2C_6H_4$)(py)}($L^A$)] (**6**) as a brown/yellow solid in 57% isolated yield; $O(SiMe_3)_2$ is produced during the reaction and provides a thermodynamic driving force (Scheme 2 Path A). Complex **6** may also be accessed by treating **1** with 2 equiv. of [HPy]Cl (Scheme 2). Complex **6** possesses two bridging chlorido ligands between the two U centres and gives rise to 13 resonances in the respective ^{1}H NMR spectrum ranging from 65.90 to −39.25 ppm. Similarly to the reactivity of **A** with XeF_2, treating **A** with 2 equiv. of Me_3SiCl at room temperature in the presence of $O(Bcat)_2$ provides a new compound that shows a broad singlet in the ^{11}B NMR spectrum at 435 ppm and 20 resonances from 100.8 to −38.30 ppm in the ^{1}H NMR spectrum at 300 K. Based on the spectroscopic data collected, the bulk product is identified as [{(py)U^{IV}(μ-Cl)(μ-OBcat)U^{IV}(μ-$O_2C_6H_4$)(py)}(L^A)] (**6A**). Unfortunately, all attempts to obtain X-ray quality crystals of **6A** led to the isolation of **6**, as **6** is the significantly more thermodynamically stable of the two. Similarly to the formation of **5** *via* **5A**, **A** is anticipated to react with 2 equiv. of Me_3SiCl and $O(Bcat)_2$ to provide **6A**, ClBcat and $O(SiMe_3)_2$. Further heating of a pyridine solution of the generated **6A** and ClBcat at 80 °C for 48 hours affords the [U^{IV}–Cl_2–U^{IV}] complex **6** and $O(Bcat)_2$ (Scheme 2 Path B).

The reactivity of **A** towards other silanes was also investigated; however, no reactions occurred with Ph_2SiH_2, Et_3SiH, Me_3SiOTf and Si_2Me_6 even after heating at 120 °C in pyridine for several days, and no reaction occurs when **A** is exposed to CO_2.

B. Solid-state structures of complexes 1–6

X-ray quality crystals of **1·3THF** were obtained by vapour diffusion of hexanes into a solution of **1** in THF at room temperature (Fig. 2A). The U–O(3) bond lengths of the bridging hydroxo ligands are 2.322(3) and 2.325(3) Å, and the U(1)–O(3)–U(1′) bond angle is 108.4(1)°, giving rise to a U⋯U separation of 3.7696(3) Å that is significantly contracted relative to **A** (3.9557(4) Å). Surprisingly, there is only one other example of a U^{IV}/U^{IV} complex bearing a bridging hydroxo ligand between the two metal centres that has been crystallographically characterised; the U–O(H) bond lengths in [K(2.2.2-crypt)] [{((^{Neop,Me}ArO)$_3$tacn)U^{IV}}$_2$(μ-O)(μ-OH)] are 2.282(3)and 2.267(3) Å (ref. 25) which are similar to those seen in **1**.

Complex **2** was crystallised by vapour diffusion of hexanes into a benzene solution at room temperature to afford [{(py)U^{IV}(μ-OMe)$_{1.69}$(μ-OH)$_{0.31}$$U^{IV}$(μ-$O_2C_6H_4$)(py)}($L^A$)]·$C_6H_6$ (**2-OMe/OH·C_6H_6**)

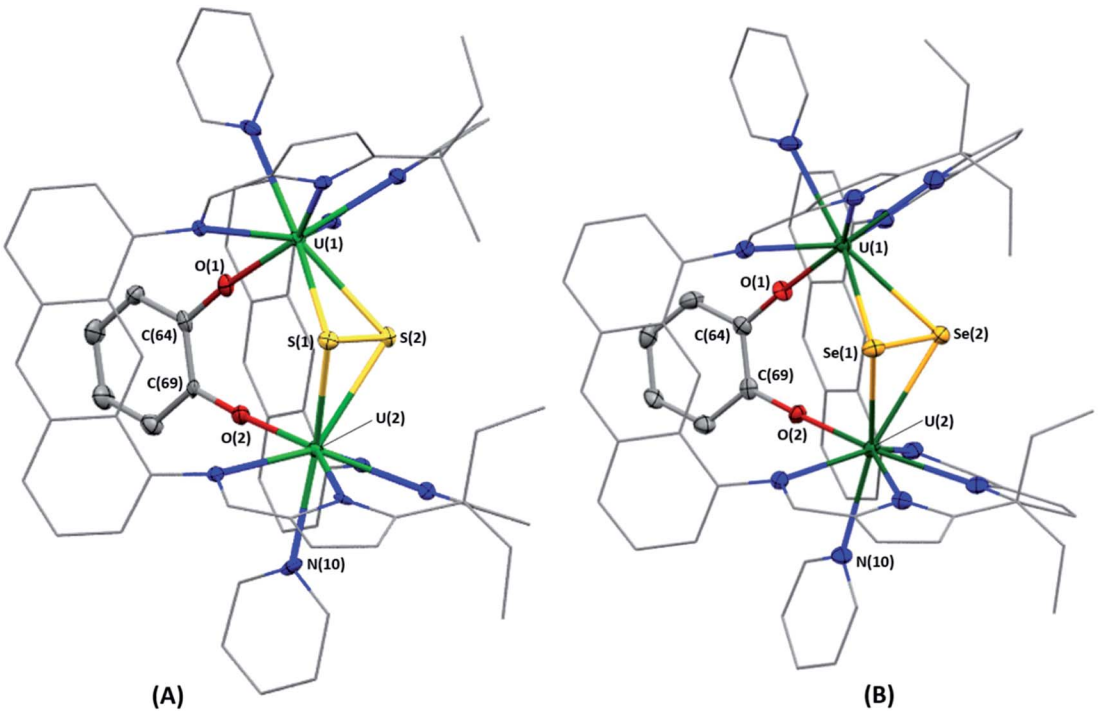

Fig. 3 Solid-state structures of **3·5py** (A) and **4·2CH_2Cl_2** (B). Displacement ellipsoids are drawn with 50% probability, and carbon atoms of L^A and U-coordinated solvent molecules drawn wireframe. For clarity, hydrogen atoms, lattice solvent and lower-fractional occupancy disorder components of one of the U-coordinated pyridine ligands in **4·2CH_2Cl_2** (N(10), C(70)–C(74)) are omitted. Selected bond lengths [Å] and bond angles [°] for **3·5py** (S(1)/S(2) refers to the centre of the bond between S(1) and S(2)): U(1)–S(1): 2.785(1); U(1)–S(2): 2.791(1); U(2)–S(2): 2.785(1); U(2)–S(1): 2.782(1); S(1)–S(2): 2.108(2); U(1)–O(1): 2.096(3); U(2)–O(2): 2.109(3); O(1)–C(64): 1.373(5); O(2)–C(69): 1.352(5); U(1)⋯U(2): 4.4194(3); U(1)–S(1)/S(2)–U(2): 118.0. Selected bond lengths [Å] and bond angles [°] for **4·2CH_2Cl_2** (Se(1)/Se(2) refer to the centroid between Se(1) and Se(2)): U(1)–Se(1): 2.9354(7); U(1)–Se(2): 2.9273(6); U(2)–Se(2): 2.9239(7); U(2)–Se(1): 2.9333(6); Se(1)–Se(2): 2.3682(9); U(1)–O(1): 2.107(4); U(2)–O(2): 2.104(4); O(1)–C(64): 1.362(7); O(2)–C(69): 1.346(7); U(1)⋯U(2): 4.5433(3); U(1)–Se(1)/Se(2)–U(2): 115.9.

Open Access Article. Published on 12 June 2020. Downloaded on 1/23/2025 2:37:06 PM.
This article is licensed under a Creative Commons Attribution-NonCommercial 3.0 Unported Licence.

in which one bridging methoxy ligand is fully occupied and the other bridging ligand has partial occupancy between a methoxy and a hydroxo ligand (Fig. 2B). Unfortunately, the partially occupied hydrogen atom of the hydroxo ligand could not be located in the difference Fourier map. The U–O(3) and U–O(4) bond lengths range from 2.345(4)–2.379(4) Å, which are elongated relative to the U^{IV}/U^{IV} bridging alkoxy complexes $K_2[\{U^{IV}\{OSi(O^tBu)_3\}_3\}_2(\mu\text{-}OCH_3)(\mu\text{-}O)(\mu\text{-}H)]$ (U–OMe = 2.30(1), 2.31(1) Å),[26] $[(^{tBu}NON)U(O^iPr)(\mu\text{-}O^iPr)]_2$ (^{tBu}NON = $O(SiMe_2N^tBu)_2$; U–O^{i}Pr = 2.33(2) Å)[27] and $[U^{IV}(COT)(S_2PPh_2)(\mu\text{-}OMe)]_2$ (U–OMe = 2.262(4), 2.348(4) Å).[28] The bridging U(1)–O(3)–U(2) and U(1)–O(4)–U(2) bond angles are 106.8(2) and 106.2(2)°, respectively, giving rise to a U···U separation of 3.7763(5) Å.

Complex **3·5py** crystallised by vapour diffusion of hexanes into a solution of **3** in pyridine at room temperature. In the solid-sate structure (Fig. 3A), the U–S bond lengths range from 2.782(1)–2.791(1) Å and are similar to those in $[\{U^{IV}(OAr)\}_2(\mu\text{-}\eta^2\text{:}\eta^2\text{-}S_2)(L^A)]$ (OAr = OC_6H_2-2,4,6-$^tBu_3$), which range from 2.707(3)–2.8229(8) Å,[29] but are significantly shorter than those in $[\{U^{IV}(Tren^{TIPS})\}_2(\mu\text{-}\eta^2\text{:}\eta^2\text{-}S_2)]$ ($Tren^{TIPS}$ = $N(CH_2CH_2NSi^iPr_3)_3$) and $[\{U^{IV}\{(SiMe_2NPh)_3\text{-}tacn\}\}_2(\mu\text{-}\eta^2\text{:}\eta^2\text{-}S_2)]$ ($(Me_2SiNHPh)_3$-tacn = 1,4,7-tris((dimethylsilyl) phenylamino)-1,4,7-triazacyclononane) which range from 2.867(1)–2.928(2) Å (ref. 30) and 2.855(2)–2.907(3) Å,[31] respectively. However, the U–S bond lengths in **3** are significantly longer than those in the U^{IV}–S–U^{IV} complexes $[\{U^{IV}\{N(SiMe_3)_2\}_3\}_2(\mu\text{-}S)]$ (2.640(4), 2.680(4) Å),[32] $[\{U^{IV}(Tren^{TIPS})\}_2(\mu\text{-}S)]$ (2.6903(6) Å)[30] and $[\{U^{IV}\{(SiMe_2NPh)_3\text{-}tacn\}\}_2(\mu\text{-}S)]$ (2.711(3), 2.703(3) Å),[31] indicating the bridging ligand in **3** is best described as a $\mu\text{-}[S_2]^{2-}$ ligand as opposed to two $\mu\text{-}S^{2-}$ ligands. The S–S distance in **3** is 2.108(2) Å, which is in good agreement with the aforementioned three U^{IV}–(S_2^{2-})–U^{IV} complexes (S–S = 2.118(3),[29] 2.104(2)[30] and 2.105(5) Å,[31] respectively). The U(1)–S(1)–U(2) and U(1)–S(2)–U(2) bond angles in **3** are 105.12(4) and 104.84(4)°, respectively, and the U(1)···U(2) separation is 4.4194(3) Å, which is significantly elongated relative to **A** and **B**,[18] and a consequence of the larger ionic radius of sulfur relative to oxygen.[33]

X-ray quality crystals of **4·2CH$_2$Cl$_2$** were obtained by diffusion of hexanes vapour into a solution of **4** in CH_2Cl_2 at room temperature, and the solid-state structure is displayed in Fig. 3B; residual electron density from highly disordered lattice solvent was removed from the structure using the "solvent mask" feature of Olex2 (84.6 electrons per unit cell, equal to 2 molecules of CH_2Cl_2). The U–Se bond lengths in **4** range from 2.9239(7)–2.9354(7) Å and the Se(1)–Se(2) bond length is 2.3682(9) Å; these compare well with $[\{((^{Ad}ArO)_3N)U^{IV}\}_2(\mu\text{-}\eta^2\text{:}\eta^2\text{-}Se_2)(\mu\text{-dme})]$ (U–Se = 2.942(1)–3.079(1) Å; Se–Se = 2.377(1) Å),[34] which also features a $[\mu\text{-}\eta^2\text{:}\eta^2\text{-}Se_2]^{2-}$ ligand between the two U^{IV} centres. Furthermore, the U–Se bond lengths in **4** are significantly longer than those reported for $[\{U^{IV}\{N(SiMe_3)_2\}_3\}_2(\mu\text{-Se})]$ (2.727(2)–2.751(2) Å),[32] $[\{((^{Ad}ArO)_3N)U^{IV}(dme)\}_2(\mu\text{-Se})]$ (U–Se = 2.830(1), 2.816(1) Å), $[\{((^{tBu}ArO)_3tacn)U^{IV}\}_2(\mu\text{-Se})]$ ($(^{tBu}ArOH)_3$tacn = 1,4,7-tris(3,5-di-*tert*-butyl-2-hydroxybenzyl)-1,4,7-triazacyclononane; 2.7188(4) Å) and $[Na(dme)_3]_2[\{((^{Ad}ArO)_3N)U^{IV}(\mu\text{-Se})\}_2]$ (U–Se = 2.819(1)–2.866(1) Å)[35] which feature bridging $[Se]^{2-}$ ligands between the two U centres, rendering the diselenide ligand in **4** best described as a bridging $[Se_2]^{2-}$ ligand. The U(1)–Se(1)–U(2) and U(1)–Se(2)–U(2) bond

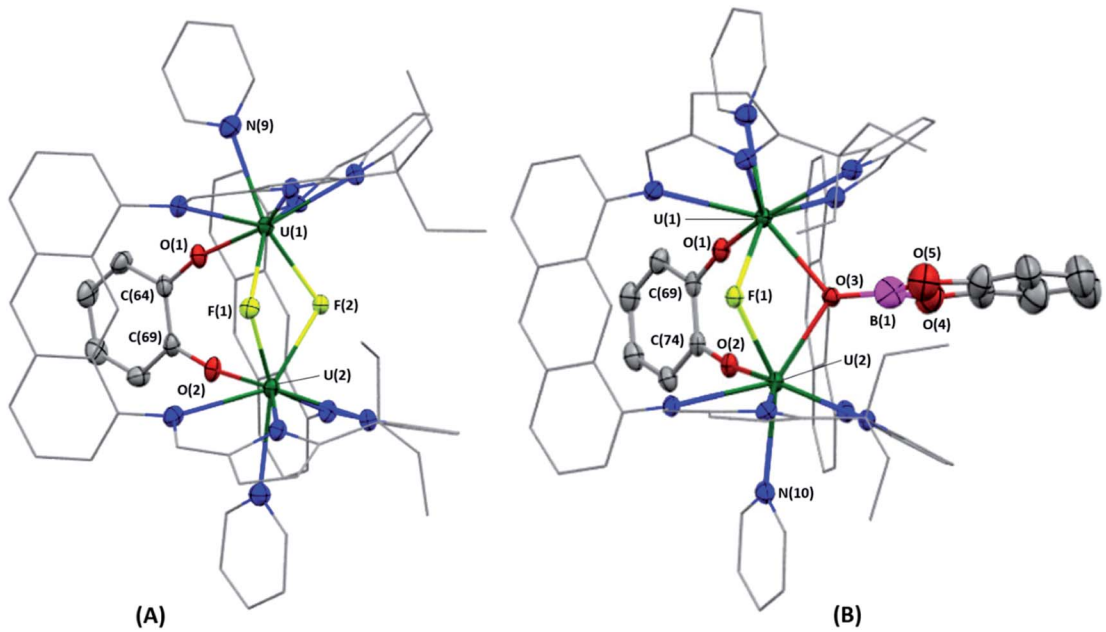

Fig. 4 Solid-state structure of **5·4py** (A) and **5A·3dme** (B). Displacement ellipsoids are drawn at 50% probability, and carbon atoms of L^A and U-coordinated solvent molecules are drawn wireframe. For clarity, hydrogen atoms and lattice solvent are omitted. Selected bond lengths [Å] and bond angles [°] for **5·4py**: U(1)–F(1), 2.391(3); U(2)–F(1), 2.299(3); U(1)–F(2), 2.307(3); U(2)–F(2), 2.382(3); U(1)–O(1), 2.120(4); U(2)–O(2), 2.106(4); O(1)–C(64), 1.347(6); O(2)–C(69), 1.362(6); U(1)···U(2), 3.8349(3); U(1)–F(1)–U(2), 109.7(1); U(1)–F(2)–U(2), 109.7(1). Selected bond lengths [Å] and bond angles [°] for **5A·3dme**: U(1)–O(1), 2.106(2); U(2)–O(2), 2.106(2); O(1)–C(69), 1.360(4); O(2)–C(74), 1.355(4); U(1)–F(1), 2.300(2); U(2)–F(1), 2.374(2); U(1)–O(3), 2.429(2); U(2)–O(3), 2.373(2); O(3)–B(1), 1.379(7); O(4)–B(1), 1.407(7); O(5)–B(1), 1.431(7); U(1)···U(2), 3.8490(2); U(1)–F(1)–U(2), 110.86(7); U(1)–O(3)–U(2), 106.53(9).

 This journal is © The Royal Society of Chemistry 2020

Open Access Article. Published on 12 June 2020. Downloaded on 1/23/2025 2:37:06 PM.
This article is licensed under a Creative Commons Attribution-NonCommercial 3.0 Unported Licence.

angles in **4** are 101.46(2) and 101.88(2)°, respectively, and the U(1)···U(2) separation is 4.5433(3) Å, which similarly to **3** is significantly greater than in **A**.

Bright yellow X-ray quality crystals of **5·4py** were grown by vapour diffusion of hexanes into a solution of **5** in pyridine at room temperature (Fig. 4A); similarly to **4·2CH$_2$Cl$_2$**, residual electron density from highly disordered lattice solvent was removed from the structure using the "solvent mask" feature of Olex2 (90.6 electrons per unit cell, equal to approximately two molecules of pyridine or one py and one hexane molecule). While all attempts to obtain X-ray quality crystals of **5A** at room temperature afforded **5**, cooling a 1,2-dimethoxyethane (dme) solution of **5A** to −20 °C for days provided **5A·3dme** as fluorescent green needles suitable for X-ray diffraction (Fig. 4B). The U–F distances in **5** and **5A** range from 2.299(3)–2.391(3) Å, which compare well with [{Cp$''_2$U^{IV}F(μ-F)}$_2$] (Cp$''$ = C$_5$H$_3$-1,3-(SiMe$_3$)$_2$) and [{Cp$''_2$U^{IV}(μ-BF$_4$)(μ-F)}$_2$], which possess U–F bond lengths of 2.297(5) and 2.343(5) Å,[36] and 2.260(5) and 2.354(5) Å, respectively.[37] The U(1)–F(1)–U(2) and U(1)–F(2)–U(2) bond angles are 109.7(1)° in **5**, whereas the U(1)–F(1)–U(2) and U(1)–O(3)–U(2) bond angles are 110.86(7)° and 106.53(9) in **5A**, respectively. The U(1)···U(2) separations in **5** and **5A** are 3.8349(3) and 3.8490(2) Å, respectively, which are contracted relative to **A** primarily due to the more acute U–X–U (X = F or OR) bond angles in **5** and **5A**.

X-ray quality crystals of **6** were obtained by vapour diffusion of hexanes into a pyridine solution of **6** at room temperature (Fig. 5); residual electron density from highly disordered lattice solvent was removed from the structure using the "solvent mask" feature of Olex2 (393.3 electrons per unit cell, equal to approximately one pyridine and seven hexane molecules). The U–Cl bond lengths range from 2.808(1)–2.826(1) Å, which compare well with [{Mes$_2$(*p*-OMePh)corrole}U^{IV}(μ-Cl)(dme)]$_2$ (U–Cl = 2.873(2), 2.840(1) Å),[38] but are elongated relative to [U^{IV}{N(SiMe$_2$^{t}Bu)$_2$}{N(SiMe$_2$^{t}Bu)(SiMe^{t}BuCH$_2$-κ^2-*N*,*C*)}(μ-Cl)]$_2$ (U–Cl = 2.799(2) Å)[39] and [(^{iPr}NON)U^{IV}Cl(μ-Cl)]$_2$ (^{iPr}NON = O{SiMe$_2$N(C$_6$H$_3$-2,6-^{i}Pr$_2$)}$_2$; U–Cl = 2.754(3) Å),[40] all of which being U^{IV}/U^{IV} complexes exhibiting a bridging-bis(chlorido) structural motif. The U(1)–Cl(1)–U(1′) and U(1)–Cl(2)–U(1′) bond angles are 95.03(5) and 95.86(5)°, respectively, and the U(1)···U(1′) separation is 4.1681(1) Å.

The U–O bond lengths to the μ-oxo ligand, U–O–U bond angles and U···U separations are 2.090(2) Å, 142.3(3)° and 3.9557(4) Å in bent **A**, respectively, and 2.139(2)/2.112(2) Å, 176.2(1)° and 4.2485(2) Å in linear **B**, respectively (Table 1).[18] In comparison, [{((^{Neop,Me}ArO)$_3$tacn)U^{IV}}$_2$(μ-O)] and [{{(^{Ad}ArO)$_3$N}U^{IV}}(μ-O)(μ-dme)] (^{Ad}ArO)$_3$N = tris(2-hydroxy-3-adamantyl-5-methylbenzyl)amine; Ad = adamantyl), which exhibit reactivity towards CO$_2$ at the μ-oxo have U–O bond lengths of 2.0869(2) and 2.1036(2) Å, U–O–U bond angles of 180.0(2)° and U···U separations of 4.174 and 4.207 Å, respectively.[14,41] Therefore, while the U–O bond lengths compare relatively well with each other, the U–O–U bond angle and U···U separation in linear **B** are more similar to the reactive U^{IV}/U^{IV} bridging oxo complexes than in **A**.

The U–O bond lengths between the U centres and the bridging dianionic catecholate ligand in complexes **1–6** range from 2.091(3)–2.139(3) Å. In addition, the C–O bond lengths within the catecholate ligand range from 1.340(5)–1.373(5) Å. Both of these are similar to those found for complex **A** (U(1)–O(1)/U(1′)–O(1′) = 2.128(3) Å; C(64)–O(1)/C(64′)–O(1′) = 1.340(6) Å),[18] supporting the assignment of complexes **1–6** as two U^{IV} centres bridged by a dianionic catecholate. The U···U separations in complexes **1–6** range from 3.7696(3) Å in **1** to 4.5433(3) Å in **4** (Table 1). This wide variation is a result of the ability of the U centre to move out of the N$_4$-plane towards the endocyclic cavity. This out-of-plane distance was found to be the greatest for complex **1**, in which U(1) and U(2) are displaced towards the centre of the molecule by 0.791 Å from their respective N$_4$-donor planes, and the smallest for complex **4**, in which the out-of-plane distances for U(1) and U(2) are 0.531 and 0.524 Å. For comparison, the non-catecholate bridged U^{IV}/U^{IV} Pacman complexes **B** (0.235, 0.467 Å), [{(py){(py)catBO}U^{IV}OU^{IV}(OBcat)(py)}(L^A)] (0.262, 0.454 Å), [{(py)(Ph$_2$HSiO)U^{IV}OU^{IV}(OSiHPh$_2$)(py)}(L^A)] (0.27 Å), [{(THF)(Ph$_2$HSiO)U^{IV}OU^{IV}(OSiHPh$_2$)(THF)}(L^A)] (0.283 Å), [{(ArO)U^{IV}(μ-η^2:η^2-S$_2$)U^{IV}(OAr)}(L^A)] (0.067 Å) and [{(ArO)U^{IV}SU^{IV}(OAr)}(L^A)] (0.034, 0.097 Å; Ar = C$_6$H$_2$-2,4,6-^{t}Bu$_3$) exhibit significantly less out-of-plane

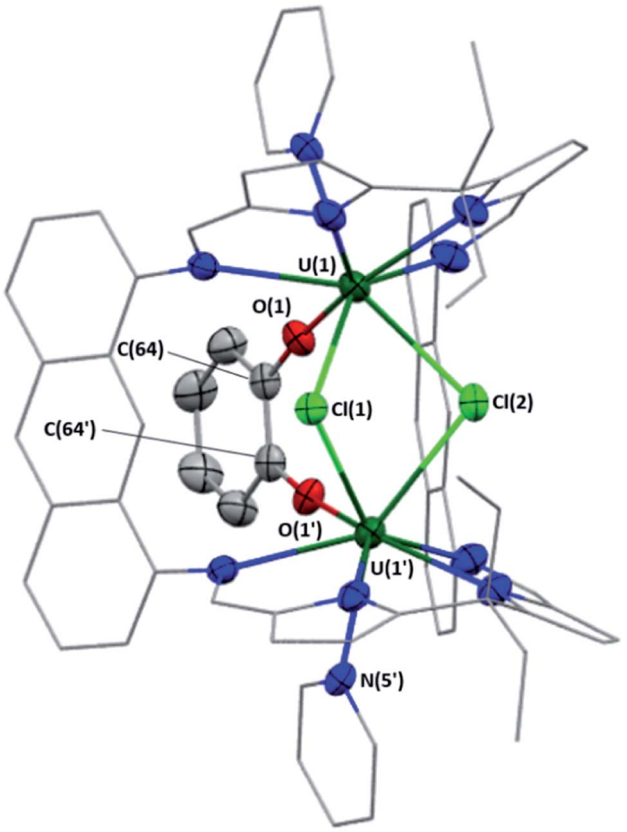

Fig. 5 Solid-state structure of **6**. Displacement ellipsoids are drawn at 50% probability, carbon atoms of L^A and U-coordinated solvent molecules are drawn wireframe. For clarity, hydrogen atoms and the lower-fractional occupancy disorder component of **6** (C(8) and one of the U-coordinated pyridine ligands, N(5), C(59)–C(63)) are omitted. Selected bond lengths [Å] and bond angles [°] for **6**: U(1)–Cl(1), 2.826(1); U(1)–Cl(2), 2.808(1); U(1)–O(1), 2.091(3); O(1)–C(64), 1.367(5); U(1)···U(1′), 4.1681(1); U(1)–Cl(1)–U(1′), 95.03(5); U(1)–Cl(2)–U(1′), 95.86(5).

Open Access Article. Published on 12 June 2020. Downloaded on 1/23/2025 2:37:06 PM.
This article is licensed under a Creative Commons Attribution-NonCommercial 3.0 Unported Licence.

Table 1 Select bond lengths and angles for complexes **A**, **B**[18] and **1–6**[a]

Complex number	**A**	**B**	**1**	**2**	**3**	**4**	**5**	**5A**	**6**
Identity of central atom(s) X	O	O	2 × OH	OH, OMe	(S_2)	(Se_2)	2 × F	F, OBcat	2 × Cl
U···U [Å]	3.9557(4)	4.2485(2)	3.7696(3)	3.7763(5)	4.4194(3)	4.5433(3)	3.8349(3)	3.8490(2)	4.1681(1)
U–X [Å]	2.090(2)	2.139(2), 2.112(2)	2.322(3), 2.325(3)	2.345(4), 2.358(5), 2.347(4), 2.379(4)	2.785(1), 2.791(1), 2.782(1), 2.785(1)	2.9354(7), 2.9273(6), 2.9333(6), 2.9239(7)	2.391(3), 2.307(3), 2.299(3), 2.382(3)	X = F: 2.300(2), 2.374(2). X = OBcat: 2.429(2), 2.373(2)	2.826(1), 2.808(1)
U(1)–O(1) [Å]	2.128(3)	N/A	2.139(3)	2.112(4)	2.096(3)	2.107(4)	2.120(4)	2.106(2)	2.091(3)
U(2)–O(2) [Å]	N/A	N/A	N/A	2.113(4)	2.109(3)	2.104(4)	2.106(4)	2.106(2)	N/A
C–O(1) [Å]	1.340(6)	N/A	1.340(5)	1.362(7)	1.373(5)	1.362(7)	1.347(6)	1.360(4)	1.367(5)
C–O(2) [Å]	N/A	N/A	N/A	1.368(7)	1.352(5)	1.346(7)	1.362(6)	1.355(4)	N/A
X–X [Å]	N/A	N/A	N/A	N/A	2.108(2)	2.3682(9)	N/A	N/A	N/A
U–X–U [°]	142.3(3)	176.2(1)	108.4(1)	106.2(2), 106.8(2)	105.12(4), 104.84(4)	101.46(2), 101.88(2)	109.7(1), 109.7(1)	X = F: 110.86(7). X = OBcat: 106.53(9)	95.03(5), 95.86(5)

[a] X refers to the bridging ligand between the two U centres.

distances of the U centres.[18,29] Such ligand flexibility, in combination with the tethering bidentate catecholate ligand allows for coordination of a wide variety of X-ligand units between the U^{IV} centres. Finally, the U–N_{imine}, U–$N_{pyridine}$ and U–$N_{pyrrolide}$ bond lengths range from 2.533(5)–2.662(3), 2.564(5)–2.645(3) and 2.441(4)–2.508(3) Å, respectively, and compare well with previously published U^{IV}-Pacman complexes.[18,42]

C. Reactivity of the linear oxo-bridged U^{IV}/U^{IV} Pacman complex, B

The μ-oxo group in **A** is very bent, U–O–U = 142.3(3)° and its substitution by larger ligating atoms forming U–S or U–Se bonds, which would normally be expected to form a weaker bond to an oxophilic uranium(IV) centre, lead us to hypothesise that the structural constraints imposed by the (μ-$O_2C_6H_4$) ligand renders the μ-oxo group reactive. To test this, we compared the reactivity of the analogous U^{IV}/U^{IV} bis(pinacolatoboroxido) complex, [{(py)(pinBO)U^{IV}OU^{IV}(OBpin)(py)}(L^A)] (**B**), which does not possess a bridging catecholate ligand, and exhibits a near linear U–O–U bonding.[18]

Reactions of **B** with XeF_2, H_2O and Me_3SiCl were carried out, and the products identified *in situ*. While **B** decomposes to [$U^{VI}O_2$(py)(H_2L^A)] and a mixture of unidentifiable species when treated with XeF_2, it reacts cleanly with 2 equiv. of H_2O to provide [{(py)HOU^{IV}OU^{IV}OH(py)}(L^A)] (**7**), as determined by ^{1}H NMR spectroscopy, giving rise to thirteen resonances between 48.23 and −34.34 ppm, diagnostic of C_{2h} symmetry. The ^{11}B NMR spectrum indicated that *H*OBpin was the sole by-product of the reaction (Scheme 3). In fact, treating **B** with 10 equiv. of H_2O produces **7** and 2 equiv. of HOBpin as the sole products, even after 24 hours at room temperature, indicating that the boroxido ligands are the preferred site of reaction over the bridging oxo ligand. Treating **B** with a slight excess of Me_3SiCl (3 equiv.) provides [{(py)ClU^{IV}OU^{IV}Cl(py)}(L^A)] (**8**), as determined by X-ray crystallography (see ESI†), and $Me_3SiOBpin$ as a reaction by-product (as determined by ^{11}B NMR spectroscopy). Unreacted Me_3SiCl, and $Me_3SiOBpin$ and $O(SiMe_3)_2$ in an approximate 6 : 1 ratio were observed in the ^{29}Si_INEPT NMR spectrum, indicating that the bridging oxo ligand in **B** possesses some reactivity towards Me_3Si^+, and a mixture of paramagnetic species were observed by ^{1}H NMR spectroscopy, a likely result of isomerisation of the coordinated chlorido ligands from axial to equatorial coordination sites (see ESI†). Conversely to treating **B** with 10 equiv. of H_2O, treating **B** with 10 equiv. of Me_3SiCl yields a mixture of products, with a nearly 1 : 1 ratio of $Me_3SiOBpin$: $O(SiMe_3)_2$ (as observed by ^{29}Si NMR spectroscopy), verifying that the boroxido and bridging oxo ligands in **B** are reactive towards Me_3Si^+.

Discussion

Complexes **1–6** are synthesised from [{(py)U^{IV}OU^{IV}(μ-$O_2C_6H_4$)(-py)}(L^A)] (**A**) and H_2O, MeOH, S_8, Se, XeF_2 and Me_3SiCl, respectively, in which the bridging oxo ligand within the bent U^{IV}–O–U^{IV} core in **A** (U–O–U = 142.3(3)°) undergoes either functionalisation or substitution. In contrast, [{(py)(pinBO)

This journal is © The Royal Society of Chemistry 2020

Open Access Article. Published on 12 June 2020. Downloaded on 1/23/2025 2:37:06 PM.
This article is licensed under a Creative Commons Attribution-NonCommercial 3.0 Unported Licence.

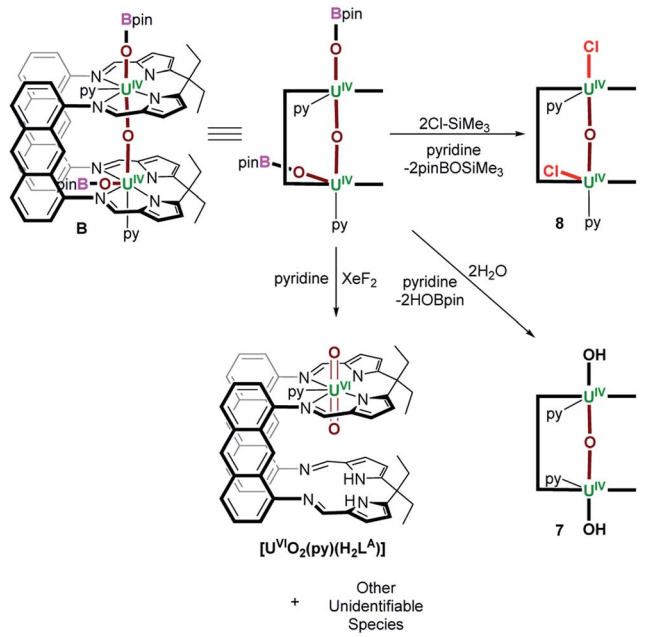

Scheme 3 Reactivity of [{(py)(pinBO)U^{IV}OU^{IV}(OBpin)(py)}(L^A)] (**B**) with XeF_2, 2 equiv. of H_2O and 2 equiv. of Me_3SiCl, providing [$U^{VI}O_2$(py)(H_2L^A)] and a mixture of unidentifiable species, [{(py)HOU^{IV}OU^{I-V}OH(py)}(L^A)] (**7**) and [{(py)ClU^{IV}OU^{IV}Cl(py)}(L^A)] (**8**), respectively.

$U^{IV}OU^{IV}$(OBpin)(py)}(L^A)] (**B**), which retains a linear U^{IV}–O–U^{IV} structure motif (U–O–U = 176.2(1)°) reacts with H_2O and Me_3SiCl to provide complexes **7** and **8**, respectively, in which reactions have occurred at the axially coordinated boroxido ligands as opposed to the μ-oxo ligand.

The reactivity of **A** with H_2O, MeOH, XeF_2 and Me_3SiCl to form complexes **1**, **2**, **5** and **6** likely occurs by initial nucleophilic attack of the μ-oxo group on the δ^+ entity of each small molecule (*i.e.* H^+, Xe^{2+} and Me_3Si^+ in H_2O/MeOH, XeF_2 and Me_3SiCl, respectively), by analogy with previous work that concluded that a nucleophilic μ-oxo group can be generated by reducing steric protection and enabling flexibility. It was noted that [{(^{Neop,Me}ArO)$_3$tacn}U^{III}], [{(^{tBu}ArO)mes}U^{III}] (^{tBu}ArOH)$_3$mes = 1,3,5-trimethyl-2,4,6-tris(2,4-di-*tert*-butyl-hydroxybenzyl)methylbenzene) and [{(^{Ad}ArO)$_3$N}U^{III}] react with CO_2 to provide the bridging $[CO_3]^{2-}$ complexes, [{{(^{Neop,Me}ArO)$_3$tacn)U^{IV}}$_2$(μ-CO_3)], [{{(^{tBu}ArO)mes}U^{IV}}$_2$(μ-CO_3)] and [{{(^{Ad}ArO)$_3$N}U^{IV}}(μ-CO_3)], respectively, *via* the initial formation of a bridging [U^{IV}–O–U^{IV}] complex followed by nucleophilic attack of the bridging oxo on CO_2.[14,41] Alternatively, [{(^{Ad,tBu}ArO)$_3$tacn}U^{III}] (^{Ad,tBu}ArOH)$_3$tacn = 1,4,7-tris(3-adamantyl-5-*tert*-butyl-2-hydroxybenzyl)-1,4,7-triazacyclononane) and [{(^{tBu}ArO)$_3$tacn}U^{III}] react with CO_2 to provide [{(^{Ad,tBu}ArO)$_3$tacn}U^{IV}(η^1-*O*CO)] and [{{(^{tBu}ArO)$_3$tacn}U^{IV}}$_2$(μ-O)], respectively, in which no further reactivity of either the [(η^1-*O*CO)]$^{1-}$ or [μ-O]$^{2-}$ ligands with CO_2 was observed.[43,44] The use of either the structurally more flexible (^{R}ArOH)$_3$mes or (^{R}ArOH)$_3$N ligand backbones, or sterically less demanding *neo*-pentyl substituents on the phenolate donors provides a more accessible, and therefore more reactive μ-oxo ligand, whereas the structurally more rigid (^{R}ArOH)$_3$tacn ligand backbone in combination with the more sterically demanding *tert*-butyl or adamantyl substituents on the phenolate donors provide protection for the μ-oxo ligand and quenches its reactivity. Here, the reactivity of **A** is enabled by the bridging dianionic catecholate ligand, which enforces a less sterically protected and bent U–O–U bond angle (142.3(3)°), and therefore more accessible and reactive bridging oxo ligand.[18] The reactivity observed can be attributed to nucleophilic attack by this oxo.

To the best of our knowledge, reactions involving **A** and elemental sulfur and selenium to provide complexes **3** and **4** are the first examples of any d- or f-block bimetallic μ-oxo complex possessing the ability to activate elemental chalcogens, which in both cases typically requires access to low valent, highly reducing metal precursors such as U^{III},[7,29–32,34] Yb^{II},[45,46] V^I/V^{III} (ref. 47 and 48) and Ni^I.[49] This reactivity sheds light on how uranium reactivity differs from the d-block and remainder of the f-block elements, and how complexes containing groups considered inert by convention can be manipulated for productive transformations.

Reactions involving **A** and S_8 or Se may proceed by one of two ways. First, similarly to the formation of complexes **1**, **2**, **5** and **6**, complex **A** may be reacting with S_8 and Se *via* initial nucleophilic attack of the bridging oxo ligand on the small molecule substrates. The [U^{IV}–E–U^{IV}] complex (E = S or Se), [{((^{Ad}ArO)$_3$N)U^{IV}(dme)}$_2$(μ-E)], formed from [((^{Ad}ArO)$_3$N)U^{III}(dme)] and either 0.125 equiv. of S_8 or 1 equiv. of selenium, have been shown to react further with either 0.125 or 0.375 equiv. of S_8, or 1 or 3 equiv. of selenium to yield [{((^{Ad}ArO)$_3$N)U^{IV}}$_2$(μ-E_2)(μ-dme)$_x$] (E = X, x = 0; E = Se, x = 1) and [{((^{Ad}ArO)$_3$N)U^{IV}}$_2$(μ-η^2:η^2-E_2)$_2$], respectively. It was reasoned that: (1) the bridging $[E]^{2-}$ ligand in [{((^{Ad}ArO)$_3$N)U^{IV}(dme)}$_2$(μ-E)] is highly nucleophilic; (2) there is reduced steric protection of the μ-E ligand through the use of a flexible amine-tethered ligand backbone; (3) the chalcogens have a propensity to catenate.[34] Alternatively, the bridging catecholate ligand could stabilise transient U^{III} centres to enable a reductive activation pathway given that it may possess three different canonical forms; (A) a dianionic catecholate, (B) a monoanionic 1,2-semiquinone, and (C) a neutral 1,2-benzoquinone (Fig. 6). Given that strongly reducing metals are typically required for the activation of elemental chalcogens,[34] resonance structures (B) and (C) could be operative in order to provide access to U^{III} centres, which would be sufficient for S_8 or Se activation (see Fig. 1B for an example of S_8 activation by a U^{III}/U^{III} complex). It is possible that S_8/Se activation may be proceeding *via* metal-based reactivity of a transient U^{III}/U^{III} or U^{III}/U^{IV} complex whereby short-lived monoanionic 1,2-semiquinone or neutral 1,2-benzoquinone resonance forms of the (μ-$O_2C_6H_4$) ligand provides an extra 1 to 2 electrons to the metal centres. Given that **A** reacts with H_2O, MeOH, XeF_2 and Me_3SiCl by nucleophilic attack of the μ-oxo ligand, and does not react with P_4, CO or CO_2, which may require redox changes in the U–cat–U (cat = catecholate) unit, we believe that the operative route to the formation of complexes **3** and **4** is by the former pathway, in which nucleophilic attack of the bridging oxo ligand on either S_8 or Se occurs initially.

An additional factor enabling conversion of **A** into complexes **1–6** is that the μ-oxo ligand may reside in a strained geometry due to the presence of a bridging catecholate ligand. This could

Open Access Article. Published on 12 June 2020. Downloaded on 1/23/2025 2:37:06 PM.
This article is licensed under a Creative Commons Attribution-NonCommercial 3.0 Unported Licence.

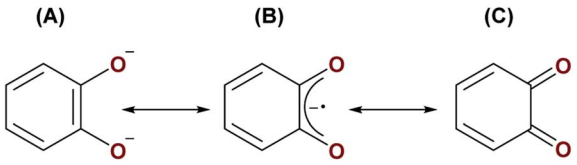

Fig. 6 Three possible resonance structures of the catecholate ligand in **A**: (A) a dianionic catecholate, (B) a monoanionic 1,2-semiquinone, and (C) neutral 1,2-benzoquinone.

be released upon ejection of the oxo group, with the new ligand bridges providing a more thermodynamically stable geometry.

The most helpful information comes from comparing the reactions of bent oxo **A** with its linear analogue **B**. While **B** reacts with H_2O and Me_3SiCl to give **7** and **8**, respectively, these reactions only take place at the axially coordinated boroxido ligands and not at the μ-oxo ligand. Overall, these results suggest that the bridging catecholate ligand plays a vital role in the formation/stabilisation of **1–6**.

In order to understand the high reactivity of complex **A**, DFT calculations (B3PW91) were carried out and the bonding situation analysed. The optimised geometry is in excellent agreement with the experimental one with the U–O bonds 2.10 Å (*vs.* 2.09 Å, Table 1), the U–O(cat) 2.13 Å (*vs.* 2.13 Å) and the U–O–U angle 144° (*vs.* 142°). Furthermore, the calculated spin density on the complexes **A** and **B** concurs with the +IV oxidation state (2.13 e^- on each uranium centre, Fig. S53†). Both indicate the suitability of the computational method to describe such a system. By scrutinising the molecular orbitals, it has been possible to locate two molecular orbitals that describe the U–O–U bonding interaction (Fig. 7).

These bonding interactions involve a sp hybrid orbital on the bridging O (91%) and a df hybrid from U (9%). Natural Bonding Orbital (NBO) analysis shows a similar bonding description, except that the bonding interaction is found to be pure donation from two sp lone pairs on the bridging O towards empty df orbitals on U (donation of 198 kcal mol^{-1}, 90% σ and 10% π, at the second order donor–acceptor; *i.e.* donation of electron density where there is no bond currently). Interestingly the Wiberg Indexes (WBI) are 0.89 for the U–O bonds (0.82 for the U–O(cat) ones) indicating strong covalent contributions to the bonding. Therefore, the U–O interactions in complex **A** are found to be covalent and overlap-driven. A similar analysis was carried out for the linear oxo complex **B** and the WBI of the U–O bond is slightly lower (0.86). In this case, the bond appears to be even more polarised toward O in complex **B** (97%) than in **A**. At the NBO level, a donation from sp orbital on O to an spdf orbital on U is found (134 kcal mol^{-1} at the second order donor–acceptor which is 70% σ and 30% π). For comparison, the U–O WBI for a bent-oxo calculated intermediate in $[\{((^{Me}ArO)_3mes)U^{IV}\}_2(\mu\text{-}O)]$, is 0.84. This intermediate is proposed to form during the reaction between $[((^{Me}ArO)_3mes)U^{III}]$ and CO_2 to yield $[\{((^{Me}ArO)_3mes)U^{IV}\}_2(\mu\text{-}CO_3)]$.[50] However, the U–O WBI for $[\{((^{Neop,Me}ArO)_3tacn)U^{IV}\}_2(\mu\text{-}O)]$, is an isolable linear oxo complex, is only 0.55.[51] Therefore, the covalency increases with the bending of the U–O–U bond angle. The presence of the two covalent U–O bonds induces the localisation of two lone pairs on O (as in a water molecule) and therefore the bending of the structure. The localisation of the lone pairs at the oxo (and its bent structure) helps categorise the reaction of the oxo with small molecules as nucleophilic since the lone pairs are ready to overlap with an incoming empty orbital, such as for example with water or methanol, and from which point the oxo is easily protonated.

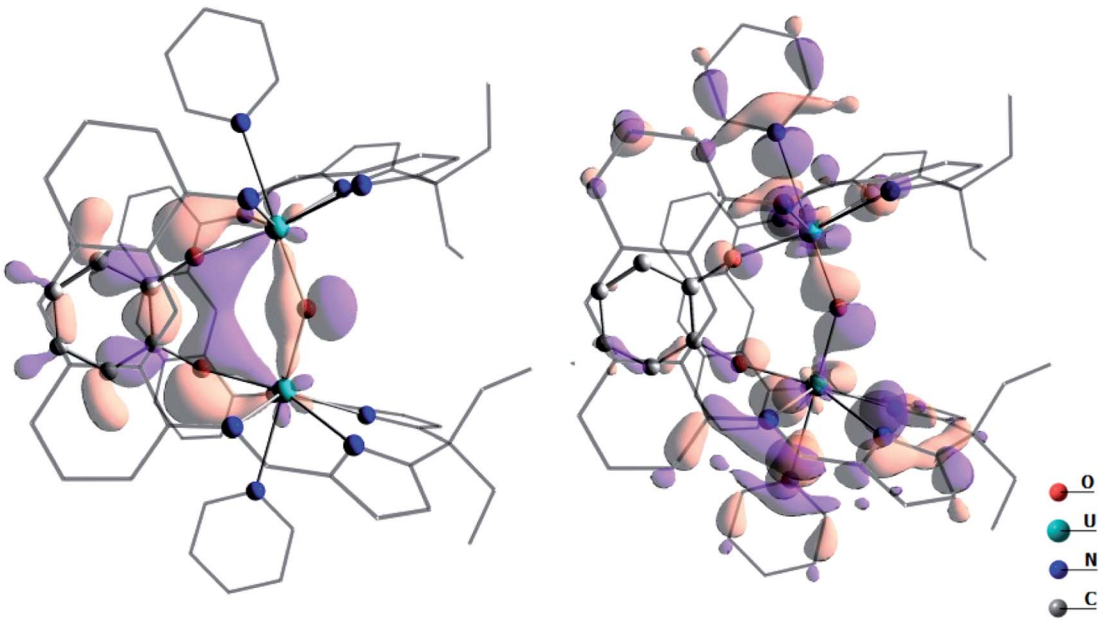

Fig. 7 Depiction of the two molecular orbitals describing the U–O bonding in complex **A**. These two orbitals are 2.42 eV lower in energy than the SOMO.

 This journal is © The Royal Society of Chemistry 2020

Open Access Article. Published on 12 June 2020. Downloaded on 1/23/2025 2:37:06 PM.
This article is licensed under a Creative Commons Attribution-NonCommercial 3.0 Unported Licence.

The presence of the catecholate ligand is also important electronically. Indeed, as can be seen on the highest energy SOMO (Fig. 8) of the system, which is mainly a linear combination of non-bonding f orbitals on the uranium centres, the π system of the catecholate stabilises the complex by counterbalancing the reduced level of π donation from the oxo.

The propensity for $[S_2]^{2-}$ and $[Se_2]^{2-}$ to displace O^{2-} during the formation of **3** and **4** is remarkable given the differences in U–O and U–S bond dissociation energies, which are 758(13)[52] and 510(63) kJ mol^{-1},[53] respectively (a value for the U–Se bond dissociation energy could not be found in the literature, but is anticipated to be even lower in energy). In light of the degree of covalency in U–μ-oxo bonding in **A**, this reversal in anticipated reactivity may be attributed to an increase in covalency and orbital overlap during coordination of the diatomic $[X_2]^{2-}$ ligands to the U centres *versus* a monoatomic X^{2-} ligand. This is further highlighted by a lack of reactivity between **A** and $Ph_3P{=}Se$, which possess P=Se and P=O (in the anticipated by-product) bond dissociation energies of 364(10) and 589(1) kJ mol^{-1},[54] respectively. The inability for $Ph_3P{=}Se$ to transfer a single Se^{2-} ligand to **A** is a consequence of a decrease in orbital overlap between the U centres and an $[Se]^{2-}$ ligand *versus* $[O]^{2-}$.

As was previously noted, the lack of reaction between **A** and CO_2 is somewhat surprising, given the propensity for the $[U^{IV}–O–U^{IV}]$ complexes $[\{((^{Neop,Me}ArO)_3tacn)U^{IV}\}_2(\mu\text{-}O)]$ and $[\{\{(^{Ad}ArO)_3N\}U^{IV}\}_2(\mu\text{-}O)(\mu\text{-dme})]$ to react with CO_2 to form $[U^{IV}–(CO_3)–U^{IV}]$ products. While the U–O bond lengths to the bridging oxo ligand in **A** are similar to those in the U(tacn) complexes, the U–O–U bond angles in these latter compounds are linear and the U⋯U separations are significantly longer and are similar those found in complex **B**. Furthermore, the longest U⋯U separation observed for complexes **1–6** is 4.5433(3) Å, whereas they are 5.275,[14] 6.277 and 5.253 Å in $[\{((^{Neop,Me}ArO)_3tacn)U^{IV}\}_2(\mu\text{-}CO_3)]$, $[\{\{(^{Ad}ArO)_3N\}U^{IV}(dme)\}_2(\mu\text{-}CO_3)]$ and $[\{((^{tBu}ArO)_3mes)U^{IV}\}_2(\mu\text{-}CO_3)]$ respectively. (Note: $[\{((^{tBu}ArO)_3mes)U^{IV}\}_2(\mu\text{-}CO_3)]$ was formed from $[((^{tBu}ArO)_3mes)U^{III}]$ and CO_2 and no isolable U^{IV}/U^{IV} μ-oxo intermediate was obtained.)[41] Therefore, while the μ-oxo ligand in **A** is both highly nucleophilic and potentially more sterically approachable due to the bent U–O–U angle caused by the μ-catecholate ligand, we suggest the lack of reactivity between **A** and CO_2 is because the short U⋯U distance is constrained by the bridging catecholate ligand.

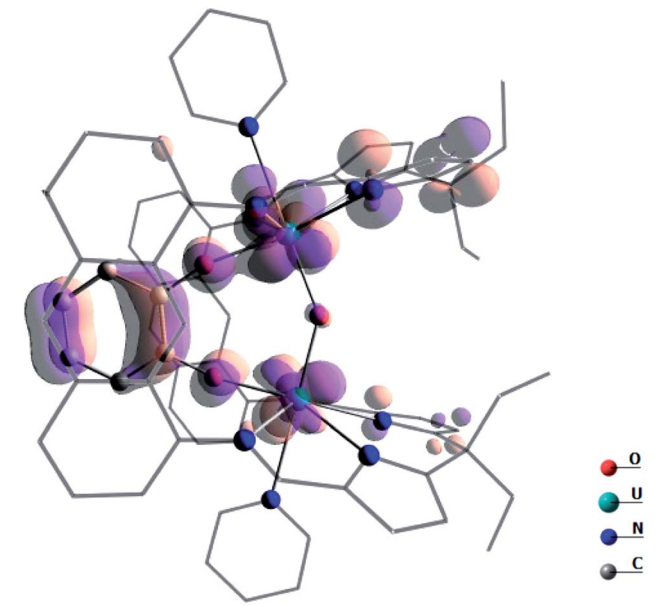

Fig. 8 Highest energy SOMO in complex **A**.

Compounds with U–O–U bond angles similarly acute to **A** include $K_2[\{OU^V(\mu\text{-}O)_2U^VO\}(L^{Me})]$ (U⋯U = 3.3795(5) Å; U–O–U = 107.5(2), 104.5(2)°), $K_2[\{O_2U^{VI}(\mu\text{-}O)U^{VI}O_2\}(L^{Me})]$ (U⋯U = 3.9762(4) Å; U–O–U = 136.4(3)°)[55] and the calculated $[\{(THF)U^{IV}OU^{IV}(THF)\}(L^{Me})]^{2+}$ (U⋯U = 3.819 Å; U–O–U = 134.0°),[56] all of which feature a smaller Pacman ligand that makes use of a phenylene hinge between the two N_4-donor pockets as opposed to an anthracenyl hinge. The complex $K_2[\{Me_3SiOU^{IV}(\mu\text{-}O)_2U^{IV}OSiMe_3\}(L^{Me})]$ was not crystallographically characterised but would be anticipated to possess similarly acute U–O–U bond angles.[55] The oxo reactivity of these synthesised complexes has not been probed.

Conclusions

The substitution of two monodentate anionic ancillary O-ligands in the linear, oxo-bridged bis(boroxido)-U^{IV}/U^{IV} Pacman complex, $[\{(py)(pinBO)U^{IV}OU^{IV}(OBpin)(py)\}(L^A)]$ (**B**) with the small bite-angle catecholate ligand in **A** causes the bending of the μ-oxo $U^{IV}OU^{IV}$ unit, and results in an increase in nucleophilicity of the oxo group. This enables a wide range of reactions that either functionalise or substitute the O atom with another functional group, including some softer ligands such as S and Se which would normally not be expected to be thermodynamically capable of this displacement. These latter transformations are to the best of our knowledge unprecedented in both d- and f-block chemistry. All of the uranium products from these reactions maintain the +4 oxidation state for both uranium centres. Computational analyses of the selective reactivity seen at the bridging oxo ligand in **A** confirms its highly nucleophilic character. There is an increase in covalency within the U–O bonds and localisation of the lone pairs of the μ-oxo ligand caused by bending the $U^{IV}–O–U^{IV}$ angle. The bridging catecholate ($\mu\text{-}O_2C_6H_4$) ligand also stabilises the resulting products of these reactions by providing additional electron donation to the U centres in order to counter balance decreased π-donation from the bridging X-ligands (X = OH, OMe, S_2, Se_2, Cl, F, OBcat). Altogether, the generation of a bent $[U^{IV}–O–U^{IV}]$ unit should enable oxo reactivity without changes in formal oxidation state. The U(III) complexes that are so famous for small molecule activation by reductive routes are also very difficult to re-reduce to close a hypothetical reaction cycle. Thus, there may be interesting new opportunities for catalytic small molecule transformations that do not require additional redox additives to achieve turnover.

Conflicts of interest

There are no conflicts to declare.

Open Access Article. Published on 12 June 2020. Downloaded on 1/23/2025 2:37:06 PM.
This article is licensed under a Creative Commons Attribution-NonCommercial 3.0 Unported Licence.

Acknowledgements

The authors thank the University of Edinburgh, the EPSRC (Grants EP/N022122/1 and EP/M010554/1), the European Commission Directorate General and Actinet JRC Userlab (ACTINET-I3-CP-CSA-JRP-232631) and the Natural Sciences and Engineering Research Council of Canada for an NSERC Post-Doctoral Fellowship (BEC). This project has received funding from the European Research Council (ERC) under the European Union's Horizon 2020 research and innovation programme (grant agreement no. 740311). Additional discussion, analysis, and writing of this manuscript (PLA) was supported by the U.S. Department of Energy (DOE), Office of Science, Office of Basic Energy Sciences, Chemical Sciences, Geosciences, and Biosciences Division at the Lawrence Berkeley National Laboratory under Contract DE-AC02-05CH1123. LM is a senior member of the Institut Universitaire de France and the Humboldt Foundation and the Chinese Academy of Science are acknowledged for support. CalMip is also gratefully thanked for a generous grant of computing time.

References

1 G. Aitken, N. Hazari, A. S. P. Frey, F. G. N. Cloke, O. Summerscales and J. C. Green, *Dalton Trans.*, 2011, **40**, 11080–11088.
2 S. M. Mansell, N. Kaltsoyannis and P. L. Arnold, *J. Am. Chem. Soc.*, 2011, **133**, 9036–9051.
3 L. Maron, O. Eisenstein and R. A. Andersen, *Organometallics*, 2009, **28**, 3629–3635.
4 J. G. Brennan, R. A. Andersen and A. Zalkin, *Inorg. Chem.*, 1986, **25**, 1756–1760.
5 L. Barluzzi, M. Falcone and M. Mazzanti, *Chem. Commun.*, 2019, **55**, 13031–13047.
6 P. L. Arnold and Z. R. Turner, *Nat. Rev. Chem.*, 2017, **1**, 1–16.
7 P. L. Arnold, L. Puig-Urrea, J. A. L. Wells, D. Yuan, F. L. Cruickshank and R. D. Young, *Dalton Trans.*, 2019, 4894–4905.
8 P. L. Arnold, *Chem. Commun.*, 2011, **47**, 9005–9010.
9 W. J. Evans and S. A. Kozimor, *Coord. Chem. Rev.*, 2006, **250**, 911–935.
10 D. E. Morris, R. E. Da Re, K. C. Jantunen, I. Castro-Rodriguez and J. L. Kiplinger, *Organometallics*, 2004, **23**, 5142–5153.
11 S. Cotton, in *Lanthanide and Actinide Chemistry*, ed. D. Woolins, B. Crabtree, D. Atwood and G. Meyer, John Wiley & Sons, West Sussex, UK, 2006, pp. 145–153.
12 N. Barros, D. Maynau, L. Maron, O. Eisenstein, G. Zi and R. A. Andersen, *Organometallics*, 2007, **26**, 5059–5065.
13 G. Zi, L. Jia, E. L. Werkema, M. D. Walter, J. P. Gottfriedsen and R. A. Andersen, *Organometallics*, 2005, **24**, 4251–4264.
14 A.-C. Schmidt, A. V. Nizovtsev, A. Scheurer, F. W. Heinemann and K. Meyer, *Chem. Commun.*, 2012, **48**, 8634–8636.
15 B. M. Gardner, J. C. Stewart, A. L. David, J. McMaster, W. Lewis, A. J. Blake and S. T. Liddle, *Proc. Natl. Acad. Sci. U. S. A.*, 2012, **109**, 9265–9270.
16 C. Camp, J. Pécaut and M. Mazzanti, *J. Am. Chem. Soc.*, 2013, **135**, 12101–12111.
17 M. Falcone, L. N. Poon, F. F. Tirani and M. Mazzanti, *Angew. Chem., Int. Ed.*, 2018, **57**, 3697–3700.
18 B. E. Cowie, G. S. Nichol, J. B. Love and P. L. Arnold, *Chem. Commun.*, 2018, **54**, 3839–3842.
19 Q.-J. Pan, S. O. Odoh, G. Schreckenbach, P. L. Arnold and J. B. Love, *Dalton Trans.*, 2012, **41**, 8878–8885.
20 P. L. Arnold, G. M. Jones, Q.-J. Pan, G. Schreckenbach and J. B. Love, *Dalton Trans.*, 2012, **41**, 6595–6597.
21 P. L. Arnold, A.-F. Pécharman and J. B. Love, *Angew. Chem., Int. Ed.*, 2011, **50**, 9456–9458.
22 R. Steudel and Y. Steudel, *Eur. J. Inorg. Chem.*, 2004, 3513–3521.
23 J. E. McDonough, A. Mendlratta, J. J. Curley, G. C. Fortman, S. Fantasla, C. C. Cummins, E. V. Rybak-Aklmova, S. P. Nolan and C. D. Hoff, *Inorg. Chem.*, 2008, **47**, 2133–2141.
24 D. S. Brock and G. J. Schrobilgen, *J. Am. Chem. Soc.*, 2011, **133**, 6265–6269.
25 A.-C. Schmidt, F. W. Heinemann, W. W. Lukens and K. Meyer, *J. Am. Chem. Soc.*, 2014, **136**, 11980–11993.
26 M. Falcone, R. Scopelliti and M. Mazzanti, *J. Am. Chem. Soc.*, 2019, **141**, 9570–9577.
27 C. E. Hayes, Y. Sarazin, M. J. Katz, J.-F. Carpentier and D. B. Leznoff, *Organometallics*, 2013, **32**, 1183–1192.
28 T. Arliguie, M. Blug, P. L. Floch, N. Mézailles, P. Thuéry and M. Ephritikhine, *Organometallics*, 2008, **27**, 4158–4165.
29 P. L. Arnold, C. J. Stevens, N. L. Bell, R. M. Lord, J. M. Goldberg, G. S. Nichol and J. B. Love, *Chem. Sci.*, 2017, **8**, 3609–3617.
30 B. M. Gardner, D. M. King, F. Tuna, A. J. Wooles, N. F. Chilton and S. T. Liddle, *Chem. Sci.*, 2017, **8**, 6207–6217.
31 C. Camp, M. A. Antunes, G. Garcia, I. Ciofini, I. C. Santos, J. Pécaut, M. Almeida, J. Marçalo and M. Mazzanti, *Chem. Sci.*, 2014, **5**, 841–846.
32 J. L. Brown, G. Wu and T. W. Hayton, *Organometallics*, 2013, **32**, 1193–1198.
33 B. Cordero, V. Gómez, A. E. Platero-Prats, M. Revés, J. Echeverría, E. Cremades, F. Barragán and S. Alvarez, *Dalton Trans.*, 2008, 2832–2838.
34 S. M. Franke, F. W. Heinemann and K. Meyer, *Chem. Sci.*, 2014, **5**, 942–950.
35 O. P. Lam, F. W. Heinemann and K. Meyer, *Chem. Sci.*, 2011, **2**, 1538–1547.
36 J. W. W. Lukens, S. M. Beshouri, L. L. Blosch, A. L. Stuart and R. A. Andersen, *Organometallics*, 1999, **18**, 1235–1246.
37 P. B. Hitchcock, M. F. Lappert and R. G. Taylor, *J. Chem. Soc., Chem. Commun.*, 1984, 1082–1084.
38 A. L. Ward, H. L. Buckley, W. W. Lukens and J. Arnold, *J. Am. Chem. Soc.*, 2013, **135**, 13965–13971.
39 C. A. P. Goodwin, F. Tuna, E. J. L. McInnes and D. P. Mills, *Eur. J. Inorg. Chem.*, 2018, 2356–2362.
40 C. E. Hayes, R. H. Platel, L. L. Schafer and D. B. Leznoff, *Organometallics*, 2012, **31**, 6732–6740.
41 O. P. Lam, S. C. Bart, H. Kameo, F. W. Heinemann and K. Meyer, *Chem. Commun.*, 2010, **46**, 3137–3139.
42 B. E. Cowie, J. M. Purkis, J. Austin, J. B. Love and P. L. Arnold, *Chem. Rev.*, 2019, **119**, 10595–10637.

 This journal is © The Royal Society of Chemistry 2020

Open Access Article. Published on 12 June 2020. Downloaded on 1/23/2025 2:37:06 PM.
This article is licensed under a Creative Commons Attribution-NonCommercial 3.0 Unported Licence.

43 I. Castro-Rodriguez and K. Meyer, *J. Am. Chem. Soc.*, 2005, **127**, 11242–11243.
44 I. Castro-Rodriguez, H. Nakai, L. N. Zakharov, A. L. Rheingold and K. Meyer, *Science*, 2004, **305**, 1757–1759.
45 D. Werner, X. Zhao, S. P. Best, L. Maron, P. C. Junk and G. B. Deacon, *Chem.–Eur. J.*, 2017, **23**, 2084–2102.
46 A. Y. Kornienko, T. J. Emge and J. G. Brennan, *J. Am. Chem. Soc.*, 2001, **123**, 11933–11939.
47 S. K. Bose, K. Geetharani, V. Ramkumar, B. Varghese and S. Ghosh, *Inorg. Chem.*, 2010, **49**, 2881–2888.
48 H.-M. Wu, Y.-H. Chang, Y.-F. Tsai, K.-F. Hsu, G.-H. Lee and H.-F. Hsu, *Dalton Trans.*, 2015, **44**, 4468–4473.
49 U. Chakraborty, F. Urban, B. Mühldorf, C. Rebreyend, B. de Bruin, N. van Velzen, S. Harder and R. Wolf, *Organometallics*, 2016, **35**, 1624–1631.
50 L. Castro, O. P. Lam, S. C. Bart, K. Meyer and L. Maron, *Organometallics*, 2010, **29**, 5504–5510.
51 A.-C. Schmidt, F. W. Heinemann, C. E. Kefalidis, L. Maron, P. W. Roesky and K. Meyer, *Chem.–Eur. J.*, 2014, **20**, 13501–13506.
52 J. Marçalo and J. K. Gibson, *J. Phys. Chem. A*, 2009, **113**, 12599–12606.
53 C. C. L. Pereira, C. J. Marsden, J. Marçalo and J. K. Gibson, *Phys. Chem. Chem. Phys.*, 2011, **13**, 12940–12958.
54 Y. R. Luo, *Comprehensive Handbook of Chemical Bond Energies*, CRC Press, Boca Raton, FL, 2007.
55 G. M. Jones, P. L. Arnold and J. B. Love, *Angew. Chem., Int. Ed.*, 2012, **51**, 12584–12587.
56 J. Yao, X.-J. Zheng, Q.-J. Pan and G. Schreckenbach, *Inorg. Chem.*, 2015, **54**, 5438–5449.